Photoionization of confined Ca in a spherical potential well

M. F. Hasoğlu,[1,2] H.-L. Zhou,[1] T. W. Gorczyca,[3] and S. T. Manson[1]
[1]*Department of Physics and Astronomy, Georgia State University, Atlanta, Georgia 30303, USA*
[2]*Department of Computer Engineering, Hasan Kalyoncu University, 27100 Sahinbey, Gaziantep, Turkey*
[3]*Department of Physics, Western Michigan University, Kalamazoo, Michigan 49008, USA*
(Received 6 October 2012; published 9 January 2013)

The photoionization cross section of the Ca atom, confined by a spherical annular potential, has been calculated using a modification to the Belfast *R*-matrix code for a variety of depths of the confining potential. The results show that the external potential affects the cross section, which is dominated by doubly excited autoionizing states, quite significantly, causing much of the oscillator strength to move into the discrete region of the spectrum. In addition, increasing well depth causes a level crossing between the first two excited states of Ca^+, thereby changing the ordering of resonances dramatically. The calculation for free Ca shows excellent agreement with experiment.

DOI: 10.1103/PhysRevA.87.013409 PACS number(s): 32.80.Fb, 31.15.xr

I. INTRODUCTION

Confined atoms are of increasing interest in connection with fundamental studies of physical systems, particularly in regard to the changes in their static and dynamic properties. They are also of applied interest to other fields of science and technology since these confined atoms are predicted theoretically to exhibit new and unique properties that are potentially relevant to a wide range of applications [1–4]. Among the important properties of confined atoms is the response of such systems to ionizing electromagnetic radiation, i.e., the photoionization process. While there have been a number of such studies (mostly theoretical) [5], the field is still in its infancy, and much remains to be learned. In addition, most of the theoretical studies model the effects of confinement, by the fullerene C_{60}, for example, using an attractive spherical potential well, which is a reasonable approximation in many cases. To get a clearer physical picture of how the confining well affects the photoionization properties of the confined atom, it is of interest to do the calculation not only for the free atom or for the atom confined by the model potential at its full depth but also for a series of intermediate depths in order to investigate the evolution of the cross section.

Since experimental results are limited, it is highly desirable to use a theoretical methodology whose results are assessable. To do that, a case should be chosen where reliable experimental and/or theoretical data exist for the free atom. Then, if the calculation agrees with experiment for the free atom, it is not unreasonable to suppose the results in the confining potential are reliable as well. Since resonances provide excellent markers to follow the evolution, an atom should be chosen for which the cross section is abundant with resonances.

The Ca atom fills the bill on both counts. The photoionization of the outer shell of neutral calcium has been studied using different methods in the past [6–8], and experimental data exist [9–11]. Three-state *R*-matrix calculations were found to be quite successful in describing the complex resonance structure endemic in outer-shell photoionization of free Ca [6]; thus, the *R*-matrix method was selected to perform the calculations. Specifically, we have carried out similar three-state *R*-matrix calculations. However, we used a somewhat more comprehensive treatment by including more states in the configuration-interaction (CI) expansions and more correlation orbitals in the basis set in order to study the response of the Ca atom. The *R*-matrix code was then modified to add the attractive well in order to study the photoionization of confined atoms [12].

II. THEORETICAL DETAILS

The processes included in the present outer-shell photoionization of Ca are given by

$$\begin{aligned} h\nu + \mathrm{Ca}(3s^2 3p^6 4s^2) &\rightarrow \mathrm{Ca}^+(3s^2 3p^6 4s\,^2S) + kp \\ &\rightarrow \mathrm{Ca}^+(3s^2 3p^6 4p\,^2P) + (ks,kd) \\ &\rightarrow \mathrm{Ca}^+(3s^2 3p^6 3d\,^2D) + (kp,kf). \end{aligned} \quad (1)$$

The *R*-matrix methodology consists of initial calculations for the N-electron Ca^+ wave functions followed by calculations for the $(N+1)$-electron bound Ca and free $e^- + Ca^+$ wave functions. Confinement effects are modeled, as in previous studies [13], via a short-range spherical potential

$$V_{\mathrm{ext}}(r) = \begin{cases} -U_0 & r_c \leqslant r \leqslant r_c + \Delta\,, \\ 0 & \text{otherwise.} \end{cases} \quad (2)$$

The inner radius of the confining potential is given by $r_c = 5.80$ a.u., the thickness of the well is $\Delta = 1.89$ a.u., and the depth of the well is increased incrementally from zero to a maximum value of $U_0 = 0.604$ Ry, corresponding to the optimized C_{60} value [14].

Since the orbitals for the N-electron wave function are obtained from the Hartree-Fock (HF) and multiconfiguration Hartree-Fock (MCHF) equations, the additional potential is included in the MCHF atomic structure codes [16] (see Chapter 4 in Ref. [15] for details) via the modification

$$\left(\frac{d^2}{dr^2} + \frac{2}{r}\{Z - [Y(nl;r) + V_{\mathrm{ext}}(r)]\} - \frac{l(l+1)}{r^2} - \varepsilon_{nl,nl}\right) \times P(nl;r) = \frac{2}{r}X(nl;r) + \sum_{n' \neq n} \lambda_{n'} P(n'l;r),$$

where $P(n'l;r)$ is a radial orbital, $Y(nl;r)$ is the sum of the direct terms, $X(nl;r)$ is the exchange term, and $\lambda_{n'}$ are off-diagonal Lagrange parameters to ensure orthogonality among

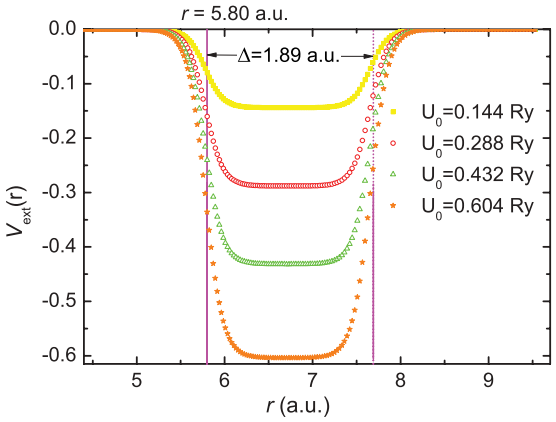

FIG. 1. (Color online) Smoothed potential wells (with $\gamma = 0.1$) plotted vs. the actual modified HF and MCHF energy mesh points.

one-electron orbitals of the same angular momentum. The MCHF code was originally designed to work with free atomic systems using logarithmic radial mesh points. However, atomic orbitals become more diffuse with the inclusion of an additional attractive potential well. Thus, further modification of the code was necessary in order to employ a finer mesh for representing these diffuse orbitals and their variations in the neighborhood of the external potential well. Lastly, in order to avoid any possible numerical difficulties arising from a steplike, discontinuous potential, a smoother Woods-Saxon-type model potential [17] is used in place of $V_{\rm ext}(r)$ in all HF and MCHF calculations, viz.,

$$V_{\rm ext}(r) \to -U_0\left[\frac{1}{1+e^{(\frac{r-r_c}{\gamma})}} - \frac{1}{1+e^{(\frac{r-[r_c+\Delta]}{\gamma})}}\right],$$

with $\gamma = 0.1$. Various smoothed potentials are shown in Fig. 1.

For the present calculations, the $1s$ through $4p$ orbitals are treated as spectroscopic and are obtained by solving the HF equations, including the appropriate potential well, for the ground state of Ca^+. The $\overline{4d}$, $\overline{4f}$, $\overline{5s}$, $\overline{5p}$, and $\overline{6s}$ pseudo-orbitals, on the other hand, are used for additional correlation and are optimized on the CI energies of the $3p^6 4p$ and $3p^6 3d$ excited states, using a frozen-core approximation for the $1s$ through $3p$ orbitals. We have found that the energy splitting between the Ca^+ $3p^6 4s$ and $3p^6 3d$ states is very sensitive to the choice of CI, a point that has also been discussed in earlier photoionization work [6]. We find that it is necessary to include configurations that have significant contribution to the $3p^6 3d$ state. We have carefully constructed our CI complexes for the N-electron target states and optimized the correlation orbitals to achieve the best agreement with the NIST energies. In order to keep the computational requirements manageable, we treat the inner $n = 1$ and $n = 2$ subshells as closed. The CI complexes for each of the $3p^6 4s$, $3p^6 4p$, and $3p^6 3d$ states are constructed by considering all possible single- and double-electron promotions consistent with (1) only single promotions out of each of the $3s$ and $3p$ subshells and (2) a maximum double occupancy of the $4p$ and $3d$ subshells. The numbers of $3p^6 3d$ and $3p^6 4p$ configurations used are 365 and 255, respectively. The $\overline{4d}$, $\overline{4f}$, $\overline{5s}$, and $\overline{5p}$ pseudo-orbitals are determined by optimizing the average term energies of the $3p^6 4s$ and $3p^6 3d$ states with relevant statistical weights of 2.0 and 10.0, respectively, and the $\overline{6s}$ pseudo-orbitals are determined by further optimization on the $3p^6 4s$ state, freezing all other orbitals.

To calculate the photoionization cross sections, we have employed the Belfast atomic R-matrix codes [18–20], with additional modifications to include the cage potential as follows (see Ref. [12] for more complete details). Given the Hamiltonian for an $(N + 1)$-electron system

$$H^{N+1} = \sum_{i=1}^{N+1}\left[-\frac{1}{2}\nabla_i^2 - \frac{Z}{r_i} + \sum_j \frac{1}{r_{ij}}\right], \tag{3}$$

the R matrix is computed from knowledge of the eigenvalues and eigenvectors of the Hamiltonian matrix, which is computed with respect to a basis ψ_α of $(N + 1)$-electron configurations:

$$\mathbf{H}_{\alpha\beta} = \langle\psi_\alpha|H^{N+1}|\psi_\beta\rangle\,. \tag{4}$$

The ψ_α are constructed from Slater determinants of one-electron basis states $u_i(r)Y_{l_i m_i}(\Omega)$, and the evaluation of the Hamiltonian matrix elements thus requires in turn the computation of one-electron and two-electron (Slater) radial integrals, the former taking the simple form

$$I_{ji} = \int_0^a u_j(r)\left[-\frac{1}{2}\frac{d^2}{dr^2} + \frac{l_i(l_i+1)}{2r^2} - \frac{Z}{r}\right]u_i(r)\,. \tag{5}$$

By including the cage potential, the total Hamiltonian is modified as

$$H^{\rm modified} = H^{N+1} + \sum_{i=1}^{N+1} V_{\rm ext}(r_i)\,, \tag{6}$$

and since the cage potential is a one-electron, spherically symmetric operator, its effect on the Hamiltonian matrix evaluation is simply to modify the one-electron integrals by the additional term

$$\begin{aligned} I_{ji}^{\rm modified} &= I_{ji} + \int_0^a u_j(r)\,[V_{\rm ext}(r)]\,u_i(r) \\ &= I_{ji} - U_0\int_{r_c}^{r_c+\Delta} u_j(r)u_i(r). \end{aligned} \tag{7}$$

Thus, the modification procedure we employ for including the cage potential simply consists of adding to every one-electron integral an additional overlap term. These integrals are easily identified in the subroutine ONEELE of the R-matrix module STG1 [19]. We note that this modification is performed for all orbitals, physical, pseudo, and continuum alike. Thus, in addition to modifying the outermost, photoionized electron, the inner atomic electrons are also affected, and thus the target state from which the outer electron scatters is modified accordingly.

The wave functions for the initial and final $(N + 1)$-electron systems are calculated using the same one-electron orbitals as for the N-electron core states, with 40 additional continuum-basis orbitals for each orbital angular momentum $l \leqslant 4$. The R-matrix radius, which encompasses all the bound orbitals, is taken to be $a = 18.1$ a.u. in the free-atom ($U_0 = 0$) case, whereas it is reduced to $a = 17.4$ a.u. for the deepest well ($U_0 = 0.604$ Ry) due to orbital contraction by the additional attractive well. The calculated ionization potential of free Ca

TABLE I. Free Ca and Ca^+ energies (Ry).

State	HF[a]	HF[b]	CI[a]	CI[b]	NIST
Ca $(3p^64s^2)$			−0.4410	−0.4479	−0.4493
Ca^+ $(3p^64s)$	0.0000	0.0000	0.0000	0.0000	0.0000
Ca^+ $(3p^63d)$	0.1524	0.1574	0.1202	0.1247	0.1247
Ca^+ $(3p^64p)$	0.2076	0.2130	0.2180	0.2303	0.2309

[a]Previous *R*-matrix results [6].
[b]Present results.

is 0.4479 Ry, in good agreement with the NIST value of 0.4493 Ry. Inclusion of the well potential increases this value to 0.6192 Ry for the deepest well.

III. RESULTS AND DISCUSSION

A. Evolution of the Ca^+ wave function with increasing well depth

The free-atom ($U_0 = 0$) wave functions for Ca^+ were first computed using HF and MCHF methods, and the resultant energies are compared to earlier *R*-matrix results [6] and NIST energies in Table I. It is seen that the present excitation and ionization energies are in excellent agreement with NIST energies. These calculations were then extended to include the potential well at increasing depths in the range $0 \leqslant U_0 \leqslant 0.604$ Ry, and the subsequent evolution of the $4s$, $3d$, and $4p$ orbitals is found to migrate from the inner atomic region to the confining potential well, as indicated in Fig. 2. Furthermore, this migration of amplitude from inner to outer regions is seen to be more prominent for the $4p$ orbital than for the $4s$ and $3d$ orbitals, and this turns out to have an important effect on the Ca^+ energy ordering and, consequently, on the photoionization cross section.

As the orbital probability amplitude migrates outward with increasing well depth, the corresponding Ca^+ energies decrease as well. This can be easily understood by considering the electron number within the well, which is defined as

$$n^* \equiv \int_{r_c}^{r_c+\Delta} |\Psi(r)|^2 \, dr \ .$$

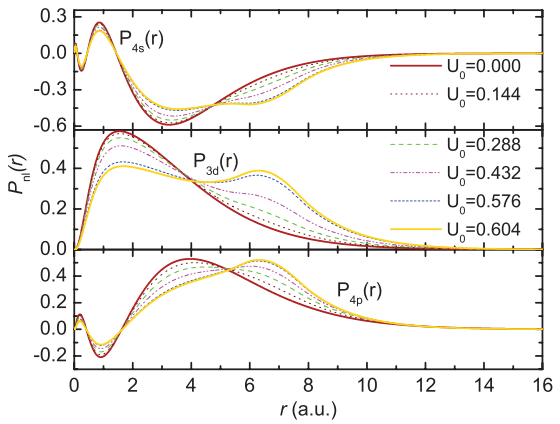

FIG. 2. (Color online) The $4s$, $3d$, and $4p$ one-electron wave functions for different values of the well depth U_0 (Ry).

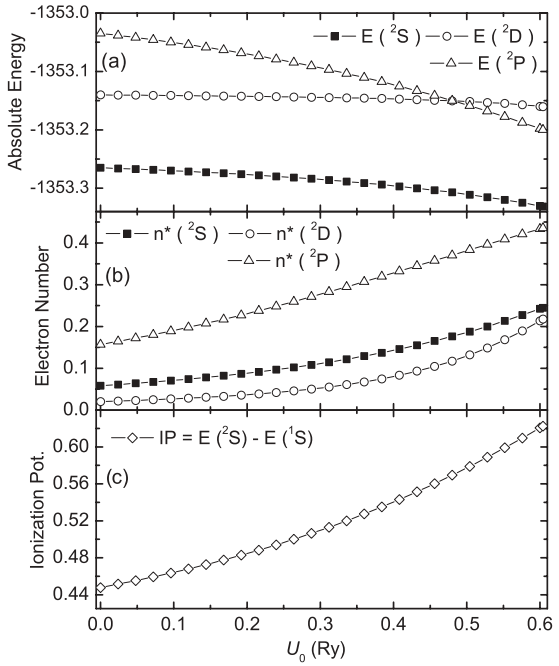

FIG. 3. Absolute energies (Ry) and electron numbers n^* for the target states and ionization potential obtained from multiconfiguration calculations as a function of depth of the confining well U_0 (Ry).

In terms of this parameter, the additional contribution to the total energy from the well is given by

$$\Delta E = \langle \Psi(r)|V_{\rm ext}(r)|\Psi(r)\rangle = -U_0 n^* \ ,$$

and thus the more rapid migration of the $4p$ state corresponds to a greater increase in n^* and therefore a greater decrease in energy, resulting in a crossing of the $3d$ and $4p$ levels, as shown in Fig. 3 and listed more quantitatively in Table II. It is also found that the Ca $3p^64s^2$ energy decreases more rapidly than the Ca^+ $3p^64s$ energy due to the lowering by the well of two $4s$ electronic energy contributions, and thus the $Ca(3p^64s^2) \rightarrow Ca^+(3p^64s)$ ionization potential increases with increasing well depth, as indicated in Fig. 3. This results in a higher-energy photoionization threshold, further changing the qualitative appearance of the photoionization cross section, as discussed below.

B. Evolution of the photoionization cross section with increasing well depth

R-matrix calculations for the free Ca atom case were performed in both length and velocity gauges; since the two results are in very good agreement, only the length results

TABLE II. Target state and ionization potential (IP) energies (Ry) as a function of U_0.

U_0	^2S	^2D	^2P	IP
0.000	0.0000	0.1247	0.2302	0.4478
0.144	0.0000	0.1310	0.2142	0.4726
0.288	0.0000	0.1397	0.1931	0.5064
0.432	0.0000	0.1519	0.1669	0.5515
0.604	0.0000	0.1711	0.1315	0.6224

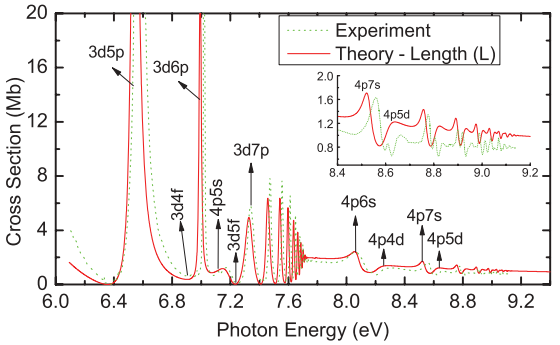

FIG. 4. (Color online) Comparison between experiment [11] and calculated photoionization cross sections for free Ca. The theoretical cross sections are convoluted with a FWHM Gaussian of 0.01 eV to simulate the experimental resolution.

are shown in Fig. 4, where they are seem to be in excellent agreement with the available experimental results [11]. This gives confidence that, using exactly the same theoretical methodology, our calculations should also be reliable for $U_0 > 0$.

To investigate how the external well affects the photoionization cross section, we have performed R-matrix calculations for gradually increasing well depths $0 \leqslant U_0 \leqslant 0.604$ Ry. These results are shown in Fig. 5, where it is clear that the confining potential alters the cross section dramatically. Both length and velocity results are shown and are in reasonably good agreement with each other, a necessary (but not sufficient) condition for calculational accuracy. With increasing depth of the confining well, the ionization threshold increases in energy. Consequently, significant oscillator strength moves into the discrete region (note the reduction of cross-section scale in Fig. 5 with increasing well depth). For example,

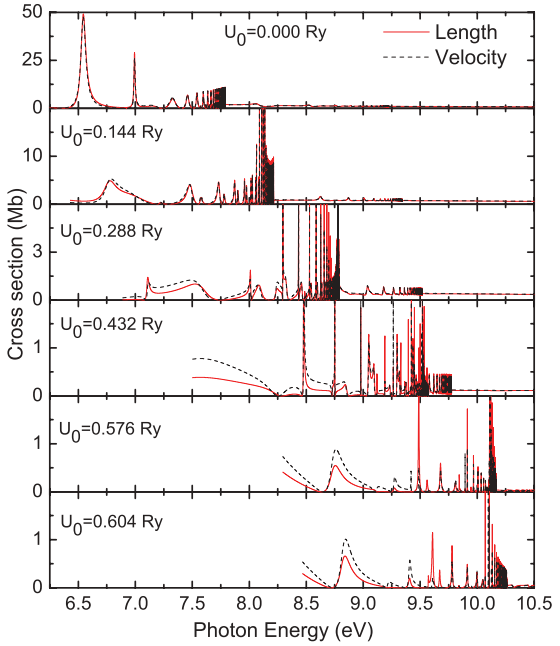

FIG. 5. (Color online) Calculated photoionization cross sections for Ca confined with varying well depths in length and velocity gauges.

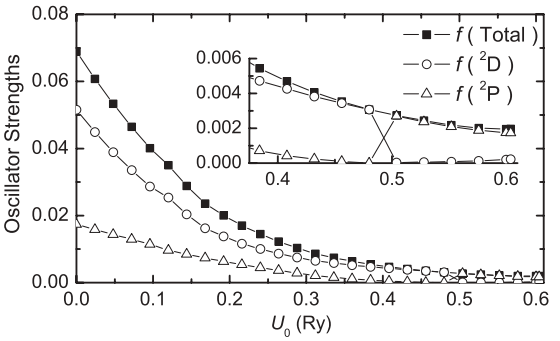

FIG. 6. Total and partial oscillator strengths in the continuum from threshold to a photon energy of 10.8 eV as a function of the well depth.

the prominent $3d5p$ resonance, which appears just above threshold for the free atom, is dramatically different for even the shallowest well. Furthermore, the region between the two excited $3d$ and $4p$ thresholds shrinks with increasing well depth, and eventually, these two states cross, as noted above. This narrowing is seen to affect the spectrum strongly; above the crossing, which includes the two deepest wells, the overall qualitative appearance of the cross section differs completely from that for the cases below the level crossing. Thus, it is evident that these doubly excited resonances are affected very strongly by the confining potential well.

Going back to the point about the movement of oscillator strength into the discrete region, with increasing well depth, it is of interest to analyze this quantitatively. The total oscillator strength in the continuum, in the region from threshold to a photon energy of 10.8 eV, has been calculated, along with the partial oscillator strengths to the excited ^2P and ^2D channels. The results are shown in Fig. 6, where the loss of continuum oscillator strength with increasing well depth is clear. The total is seen to drop by roughly an order of magnitude from the free atom to the deepest well case. This puts a quantitative face on the qualitative observation made in connection with Fig. 5. Further, the inset shows that the oscillator strengths of the ^2P and ^2D excited channels switch values when the crossing occurs.

To show in more detail what occurs with the advent of the external potential well, the cross section for the deepest well, $U_0 = 0.604$ Ry, is shown in Fig. 7 with the resonances

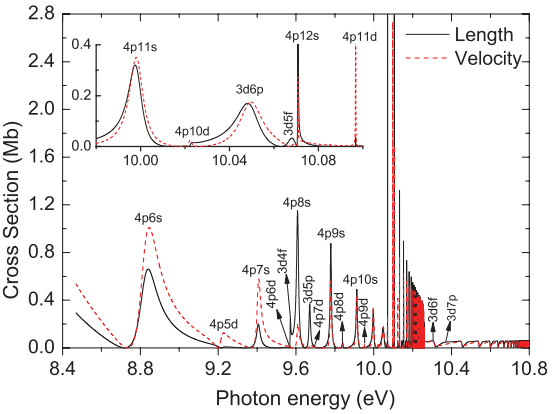

FIG. 7. (Color online) Photoionization cross section for Ca confined with $U_0 = 0.604$ Ry.

analyzed. Comparing these results to the free atom case shown in Fig. 5 reveals that a number of resonances are missing from the confined cross section. In addition, owing to the level crossing of the ^2P and ^2D states of Ca^+, the order of the resonances changes completely, thereby explaining why the cross sections for well depths above the crossing look so different from those below the crossing.

We have also analyzed the computed resonances of Ca confined in the deepest well ($U_0 = 0.604$ Ry) using the QB program [21,22]. Those resonances which have been identified in the cross-section profile are shown in Fig. 7 and are to be contrasted with the resonance identifications and orderings in Fig. 4 for the free atom.

IV. CONCLUSION

The near-threshold photoionization cross section of a Ca atom, located at the center of a spherical annular potential well, is found to change significantly from the free Ca result. The threshold energy increases with well depth, and much of the oscillator strength, as well as the lower-energy resonances themselves, moves into the discrete region. In addition, a level crossing, as a function of well depth, changes the resonance spectrum dramatically. Since there is nothing special about Ca, it is likely that these effects will ensue for any atom whose spectrum is dominated by doubly excited resonances, as well as those with low-lying excited states of the ion.

These calculations were performed with a version of the Belfast *R*-matrix code [12]. These same codes were also used for the photoionization of free Ca, giving quite good agreement with experiment: the most accurate theoretical results on the near-threshold photoionization of free Ca reported to date. The advantage of using the *R*-matrix methodology for studying the effects of confinement is that this method is much more versatile than some of the other methods that have been brought to bear on the problem; specifically, the *R*-matrix method applies equally well to open- and closed-shell atoms, and furthermore, both doubly excited states and ionization plus excitation can be included. We are currently at work on applying the *R*-matrix method to other confined systems.

ACKNOWLEDGMENTS

This work was supported by the DOE, Office of Chemical Sciences, NSF, and NASA.

[1] H. Shinohara, Rep. Prog. Phys. **63**, 843 (2000).
[2] A. L. Buchachenko, J. Phys. Chem. B **105**, 5839 (2001).
[3] L. Forró and L. Mihály, Rep. Prog. Phys. **64**, 649 (2001).
[4] P. Moriarty, Rep. Prog. Phys. **64**, 297 (2001).
[5] V. K. Dolmatov, in *Advances in Quantum Chemistry: Theory of Quantum Confined Systems*, edited by J. R. Sabin and E. Brandas (Academic, New York, 2009), pp. 13–68, and references therein.
[6] P. Scott, A. E. Kingston, and A. Hibbert, J. Phys. B **16**, 3945 (1983).
[7] C. H. Greene and L. Kim, Phys. Rev. A **36**, 2706 (1987).
[8] S. Benec'h and H. Bachau, J. Phys. B **37**, 3521 (2004).
[9] G. H. Newsom, Proc. Phys. Soc. **87**, 975 (1966).
[10] V. L. Carter, R. D. Hudson, and L. L. Breig, Phys. Rev. A **4**, 821 (1971).
[11] U. Griesmann, N. Shen, J.-P. Connerade, K. Sommer, and J. Hormes, J. Phys. B **21**, L83 (1988).
[12] T. W. Gorczyca, M. F. Hasoglu, and S. T. Manson, Phys. Rev. A **86**, 033204 (2012).
[13] J.-P. Connerade, V. K. Dolmatov, and S. T. Manson, J. Phys. B **32**, L395 (1999).
[14] Y. B. Xu, M. Q. Tan, and U. Becker, Phys. Rev. Lett. **76**, 3538 (1996).
[15] C. Froese Fischer, T. Brage, and P. Jonsson, *Computational Atomic Structure: An MCHF Approach* (IOP Publishing, Bristol, UK, 1997).
[16] C. Froese Fischer, G. Tachiev, G. Gaigalas, and M. R. Godefroid, Comput. Phys. Commun. **176**, 559 (2007).
[17] R. D. Woods and D. S. Saxon, Phys. Rev. **95**, 577 (1954).
[18] P. G. Burke, *R-Matrix Theory of Atomic Collisions* (Springer, New York, 2011).
[19] K. A. Berrington, W. Eissner, and P. N. Norrington, Comput. Phys. Commun. **92**, 290 (1995).
[20] W. Eissner, M. Jones, and H. Nussbaumer, Comput. Phys. Commun. **8**, 270 (1974).
[21] L. Quigley and K. Berrington, J. Phys. B **29**, 4529 (1996).
[22] K. Berrington, L. Quigley, and J. Pelan, Comput. Phys. Commun. **114**, 225 (1998).